J. Fluid Mech. (2017), *vol.* 825, *pp.* 16–28.
doi:10.1017/jfm.2017.376

Aeration of water with oxygen microbubbles and its purging effect

Tatsuya Yamashita[1] **and Keita Ando**[1,†]

[1]Department of Mechanical Engineering, Keio University, Yokohama 223-8522, Japan

(Received 6 May 2016; revised 4 March 2017; accepted 26 May 2017;
first published online 19 July 2017)

In this paper, we apply aeration with oxygen microbubbles to tap water; the intent is to quantitatively evaluate whether nitrogen gas originally dissolved in the water under the atmosphere is purged by the aeration with oxygen microbubbles. Oxygen microbubbles are continuously injected into the circulation system of tap water open to the atmosphere. While the concentration of dissolved oxygen (DO) can be detected by a commercial DO meter, that of dissolved nitrogen (DN) is unavailable. To detect the DN level, we observe the growth of millimetre-sized gas bubbles nucleated at glass surfaces in contact with the aerated water and compare it with the multi-species theory of Epstein and Plesset where the (unknown) DN concentration is treated as a fitting parameter. In the theory, we solve binary diffusion of each gas species (oxygen or nitrogen) in the water independently, under the assumption that the dissolved gases are sufficiently dilute. Comparisons between the experiment and the theory suggest that the DN in the water is effectively purged by the oxygen aeration. The supplemental experiment of aeration with nitrogen microbubbles is also documented to show that the DO can be effectively purged as well.

Key words: bubble dynamics, drops and bubbles

1. Introduction

Aeration is employed to efficiently control the amount of gases dissolved in water with various purposes. To enhance the rate of gas dissolution, we often use bubbling where smaller-sized gas bubbles (with larger Laplace pressure and longer residence time) (Takahashi 2005) are favoured. There are various techniques to generate micrometre-sized bubbles (the so-called microbubbles) based on decompression, hydrodynamic cavitation or membrane filtration, for example (Khuntia, Majumder & Ghosh 2012). Aerated water in which gases dissolve beyond their saturation levels has potential uses for industrial and medical purposes, including wastewater treatment (Terasaka *et al.* 2011), ozonation for disinfection (Kobayashi *et al.* 2011), hydroponics (Ebina *et al.* 2013), cultured fishery (Endo *et al.* 2008) and a rapid oxygen delivery system in therapeutics (Creech *et al.* 2002). To suppress oxidation in food processing, it is favourable to replace oxygen gas with an inert gas such as nitrogen or argon (Butler, Schoonen & Rickard 1994; Tsuge 2014). On the contrary, nitrogen gas should be purged to avoid decompression sickness of marine divers (Goldman 2007)

† Email address for correspondence: kando@mech.keio.ac.jp

or gas-bubble disease in fish (Bouck 1980) as a result of the formation of nitrogen bubbles in blood or tissues. In these applications, it is essential to quantitatively monitor gas dissolution in liquids.

While the concentration of dissolved oxygen (DO) in the aerated water can be detected by a commercial DO meter, there do not exist commercially available sensors to detect that of dissolved nitrogen (DN). To detect the DN level, which is the target of the present study, we observe the growth of millimetre-sized gas bubbles nucleated at glass surfaces in contact with aerated water and compare it with the extended theory of Epstein & Plesset (1950) that predicts quasi-static growth or dissolution of a single gas bubble whose translation under buoyancy is ignored. The original theory considers the case of single gas species dissolved in liquids. When it comes to discussing the case of air in water, the binary diffusion rates of DO and DN are of the same order, so that air is usually treated as single-species molecules (Kabalnov *et al.* 1998; Shim *et al.* 2014). For observing quasi-static bubble growth, Enríquez *et al.* (2013, 2014) used water–CO_2 solutions with other gas species (air) expelled in order to ignore any interaction between the different gases. In recent studies (Holocher *et al.* 2003; Kwan & Borden 2010; Dalvi & Joshi 2015; Peñas-López, Parrales & Rodríguez-Rodríguez 2015; Yasui, Tuziuti & Kanematsu 2016), the classical Epstein–Plesset theory is extended to account for binary diffusions of different gas species dissolved in a liquid for the case of subsaturation or saturation under which bubbles dissolve into the liquid. In these studies, dissolved gas species can be assumed to be dilute enough to ignore their interaction, which allows one to rely on Henry's law that indicates a linear proportionality between dissolved gas concentration and gas partial pressure at bubble interfaces. As a result, it is possible to solve the diffusion equation for the different gas species independently. Finally, we note a recent advance in the Epstein–Plesset type analysis that accounts for a history effect (Peñas-López *et al.* 2016); when the concentration of dissolved gases at bubble interfaces varies in time, the mass transfer into bubbles depends on its history in past times. Even under static ambient pressure, such a history effect can in principle arise due to the action of surface tension but is negligible for micrometre-sized or even larger bubbles (Chu & Prosperetti 2016), which are our target in the present experiments.

In this study, we aim to quantitatively evaluate whether nitrogen gas originally dissolved in water under one atmosphere is purged by the aeration with oxygen microbubbles. Oxygen microbubbles are continuously injected into the circulation system of tap water open to the atmosphere. The DO concentration is monitored using a DO meter of fluorometric type. To detect the DN level, we observe diffusion-driven growth of a gas bubble nucleated at glass surfaces in contact with the aerated water and compare it with the multi-species theory of Epstein and Plesset that accounts for the binary diffusion of DN in addition to DO (Kwan & Borden 2010; Yasui *et al.* 2016) and treats the (unknown) DN concentration as a fitting parameter. The supplemental experiments of the aeration with nitrogen microbubbles are also documented in the appendices.

2. Experiments

2.1. *Aeration and DO measurement*

Tap water that is originally saturated with air at room temperature (approximately 19 °C) and ambient pressure (1 atm) is aerated using a commercially available, microbubble generator of spiral flow type (Japan Patent No. 2011-088079), which is depicted in figure 1(*a*). This bubble generator creates swirling liquid flow at the

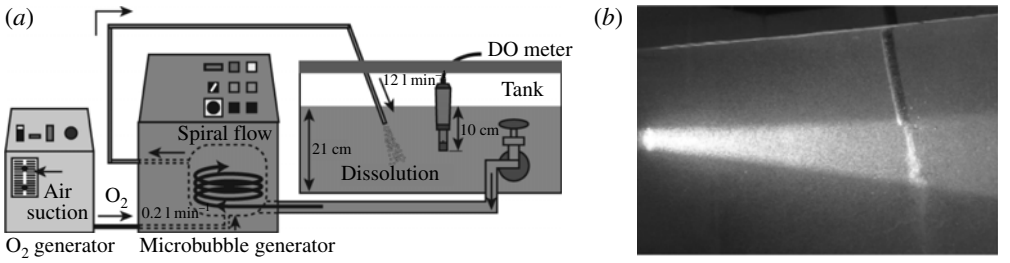

FIGURE 1. (*a*) A schematic diagram of aerating water by a commercial microbubble generator of spiral flow type. The O_2 generator is replaced with an N_2 generator in supplemental experiments (documented in the appendices). (*b*) Image of the aeration with oxygen microbubbles produced by the commercial microbubble generator. Oxygen bubbles are ejected from a polyurethane tube whose inner and outer diameter are 7 mm and 9.5 mm, respectively.

volume flow rate of 12 l min^{-1} driven by a centrifugal pump whose rotation core shows a pressure reduction due to centrifugal effects. Pure oxygen gas is sucked into the low-pressure region at the volume flow rate of 0.2 l min^{-1}; the gas phase is split into micrometre-sized oxygen bubbles due to shearing or compression under pressure recovery (Uesawa *et al.* 2012). Analyses of bubble images captured by a high-speed camera with a microscope show that the most probable radius of the bubbles is found to be approximately 50 μm. As seen in figure 1(*b*), light from a light-emitting diode (LED; SLG-150V, Revox) is scattered due to a large number of microbubbles that float in the water. Tap water in a 39.6 l acrylic tank open to the atmosphere is circulated by the pump through the bubble generator. Temperature and DO concentration (10 cm from the free interface) are monitored by a DO meter with a fluorometric sensor (SG9, Mettler Toledo). Here, we define the (dimensionless) supersaturation of DO according to

$$\zeta_1 = \frac{c_1 - c_{s,1}(T)}{c_{s,1}(T)}, \tag{2.1}$$

where c_1 is the DO concentration detected by the DO meter (in mass per unit volume) and $c_{s,1}$ is the saturated DO concentration at water temperature T. Note that the subscript 1 indicates oxygen while the subscript 2 will be used for nitrogen in the following analysis; the supersaturation of DN, ζ_2, is defined in the same manner. For reference, the saturated concentrations of DO and DN under the atmospheric pressure (0.2 atm oxygen and 0.8 atm nitrogen) are $c_{s,1} = 9.09$ mg l^{-1} and $c_{s,2} = 16.4$ mg l^{-1}, respectively, from Henry's law that suggests a linear proportionality between dissolved gas concentration and gas partial pressure at free surfaces. Since the amount of other dissolved gases such as argon is very small, we account for contributions from oxygen and nitrogen only. During the aeration, a temperature rise due to pumping effects was up to 4 °C.

A maximum (or steady-state) value of DO supersaturation ζ_1 is achieved approximately 30 min after the aeration starts; it records $\max(\zeta_1) = 6.0$ in the experiment. After the aeration is finished, large bubbles escape from the tank by buoyancy and the water again looks transparent like usual tap water. For the case of carbonated beverages, gas supersaturation is created by a sudden pressure reduction after pressurized bottles are opened to the atmosphere. Pressure waves accompanied

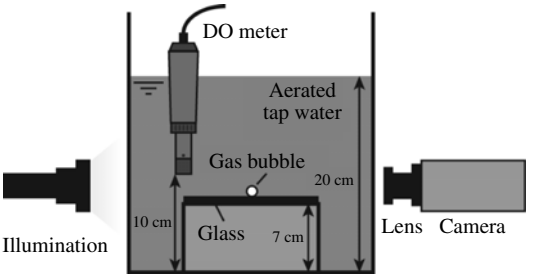

FIGURE 2. A schematic diagram of visualizing the growth of a bubble nucleated at a glass surface in the aerated water.

by the bottle opening propagate inside the liquid and are expected to work as a mechanical disturbance to activate nucleation sites at bottle surfaces. Bubbles form from a number of activated nucleation sites, continue to grow under supersaturation, and are eventually detached from bottle surfaces by buoyancy. On the other hand, the water aerated with microbubbles is put under the atmosphere and is not subjected to such a pressure transient. Indeed, the bubble formation at the container surface is found to be rather sporadic in comparison to carbonated beverages. This might be attributed to smaller population of activated nucleation sites in the aerated water. The supersaturation in the aerated water decays over several days as the DO gradually escapes, with a limited number of nucleation sites, through the free surface. The lower DO supersaturation level is prepared simply by leaving the water open to the atmosphere.

2.2. *Observation of bubble growth under supersaturation*

We observe the growth of a bubble nucleated in the aerated water, which is transferred from the water tank (figure 1) to a 12.5 l glass container, as illustrated in figure 2. To heterogeneously trigger bubble nucleation, a microscope glass slide on which a crack of approximately 100 μm radius is intentionally created by a glass cutter is inserted in the water. Now that the water is supersaturated with DO, a bubble nucleated from the crack is expected to grow as the DO is transferred into the bubble. The bubble growth driven by the mass diffusion is recorded with a video camera (Ultra Cam, nac) with a microscope (×5.5–6.5, 7.6–9.1 μm per pixel) at two frames per minute until it detaches from the surface with buoyancy defeating the capillary force. The time for bubble detachment varies between different observations, as will be seen in figures 5(*a*) and 6(*a*), for the nucleation site created by a glass cutter is believed to have rough surfaces. Since the inception of bubble nucleation is an instant event, it is an experimental challenge to capture it. We found in the video a nucleated bubble from the crack within a couple of minutes after inserting the glass slide into the water. Practically, we define time $t = 0$ at the initial video frame to capture the nucleated bubble, for the time to find the nucleation was much shorter than the bubble growth phase. The bubble image is extracted by thresholding based on Otsu's method (Otsu 1979).

The observation was performed at four different conditions (i)–(iv) of initial bubble radius R_0 and DO supersaturation ζ_1 (see table 1). We confirmed that the DO reading ζ_1 remained unchanged during the observation of the bubble growth. The observed bubble growth is to be compared with the multi-species Epstein–Plesset calculation where the (unknown) DN supersaturation is treated as a fitting parameter.

Experimental condition	(i)	(ii)	(iii)	(iv)
Initial bubble radius, R_0 (μm)	235	317	379	375
DO supersaturation (measured), ζ_1	6.0	5.4	2.9	1.8
DN supersaturation (fitted), ζ_2	−0.91	−0.9	−0.37	−0.22

TABLE 1. Initial radius of the nucleated bubble (captured in the initial frame), supersaturation from the DO reading, and fitted values of DN supersaturation in experiments (i)–(iv).

3. Multi-species theory of Epstein and Plesset

Assuming that bubble growth driven by mass diffusion in a supersaturated solution is gradual enough to ignore advection effects (and that there are no boundaries in the vicinity of bubbles of concern), mass transfer at spherical bubbles can be modelled by the diffusion equation with spherical symmetry. Epstein & Plesset (1950) derived the formula of the quasi-static growth rate of a spherical bubble in infinite liquids for the case of single gas species:

$$R\frac{\mathrm{d}R}{\mathrm{d}t} = \frac{D}{\rho_G}\frac{\left[c_\infty - c_s\left(1+\dfrac{2\gamma}{Rp_\infty}\right)\right]}{\left(1+\dfrac{4\gamma}{3Rp_\infty}\right)}\left(1+\frac{R}{\sqrt{\pi Dt}}\right), \tag{3.1}$$

where R is the bubble radius, D is the binary diffusion coefficient, ρ_G is the gas density inside the bubble, γ is the surface tension, p_∞ is the ambient pressure (for this study, one atmosphere) and c_∞ and c_s stand, respectively, for the undisturbed concentration away from the bubble and the saturated concentration corresponding to p_∞. Vapour pressure at room temperature is much smaller than gas pressure inside the bubble and its contribution is thus neglected in (3.1). Our target is the case of supersaturation (i.e. $c_\infty > c_s$) under which bubbles will grow due to gas influx. As the bubble grows, surface tension becomes less influential; this assumption is reasonable, for the bubble size of our concern is of the order of submillimetres to millimetres. Under the approximations, the Epstein–Plesset theory can be extended to include the two components of pseudo-binary gases (Kwan & Borden 2010):

$$\frac{\mathrm{d}R}{\mathrm{d}t} = \frac{BT}{4\pi R^2 p_\infty}\sum_{i=1}^{2}\frac{\mathrm{d}n_i}{\mathrm{d}t}, \tag{3.2}$$

where B is the universal gas constant, n_i is the number of moles of gas species i inside the bubble and T is the (undisturbed) room temperature. Note that $i=1$ and 2 stand for oxygen and nitrogen, respectively, which we model as ideal gases; the atmospheric pressure p_∞ consists of $p_{\infty,1} = 0.2$ atm from oxygen gas and $p_{\infty,2} = 0.8$ atm from nitrogen gas. The molar transfer rate for species i is governed by Fick's law together with Henry's law:

$$\frac{\mathrm{d}n_i}{\mathrm{d}t} = 4\pi R^2 D_i K_{H,i}[p_{\infty,i}(\zeta_i+1) - p_i]\left(\frac{1}{R}+\frac{1}{\sqrt{\pi D_i t}}\right), \tag{3.3}$$

where $K_{H,i}$ is the Henry's constant of species i and $p_i = n_i BT/(4\pi R^3/3)$ is the partial pressure of species i inside the bubble. The right-hand side of (3.3) divided

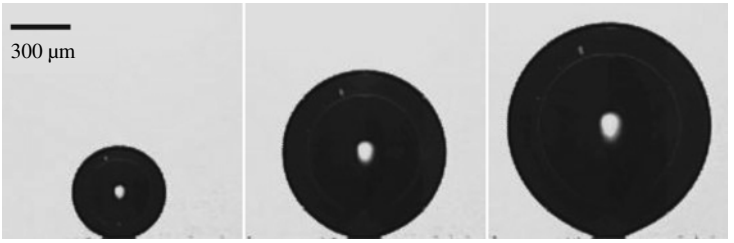

FIGURE 3. A growing bubble attached at the glass surface in experiment (i) under the (maximum) supersaturation of DO at $\zeta_1 = 6.0$. The image at $t = 0$ corresponds to the initial video frame to capture the nucleated bubble.

by $4\pi R^2 D_i$ represents the concentration gradient at the bubble wall, $(\partial c_i/\partial r)|_{r=R} = (c_{\infty,i} - c_{s,i})(1/R + 1/\sqrt{\pi D_i t})$ (Duncan & Needham 2004; Peñas-López *et al.* 2015). The binary diffusion coefficients (in water) and the Henry's constants of species $i = 1$ and 2 are obtained from Wilhelm, Battino & Wilcock (1977) and Sander (2015): $D_1 = 2.4 \times 10^{-9}$ m^2 s^{-1}, $D_2 = 2.0 \times 10^{-9}$ m^2 s^{-1}, $K_{H,1} = 1.2 \times 10^{-5}$ mol m^{-3} Pa^{-1} and $K_{H,2} = 6.4 \times 10^{-6}$ mol m^{-3} Pa^{-1}.

It is possible to extend the Epstein–Plesset theory to the case of spherical bubbles attached at hydrophilic surfaces with very small contact angles such as glasses. As we will see (in figure 3), the bubble we obtained remains fairly spherical during the observation. This situation can be modelled by considering an imaginary bubble (of identical size) mirrored at the opposite side of the glass surface in order to satisfy the no-penetration condition across the solid boundary. This means that the bubble growth is hindered by having the imaginary bubble. According to Enríquez *et al.* (2014), the effective area ($4\pi R^2 f_{A,i}$) through which mass transfer of species i occurs is estimated by introducing the (dimensionless) geometric correction factor:

$$f_{A,i} = 1 - \frac{1}{2}\frac{\sqrt{\pi D_i t}}{R + \sqrt{\pi D_i t}}. \tag{3.4}$$

The asymptotic limit $f_{A,i} \to 0.5$ means that the concentration boundary layer develops fully and becomes much larger than the bubble, so that the mass transfer rates halve. For comparisons with the experiments, (3.2) and (3.3) together with correction factor $f_{A,i}$ from (3.4) are integrated numerically by the ordinary differential equation (ODE) solver ode45 of MATLAB. In these equations, while DO supersaturation ζ_1 is taken from the DO reading in the experiments, DN supersaturation ζ_2 is unknown and thus treated as a fitting parameter.

When it comes to evaluating the developing concentration boundary layer whose thickness is estimated by $\sqrt{\pi D_i t}$ in (3.3) and (3.4), the time t needs, ideally speaking, to be measured from the instant of bubble nucleation, which cannot be observed from the experiments. While we find nucleated bubbles, say, one minute after the glass slide is inserted into the aerated water, the boundary layer has already developed from bubble interfaces and its extent is estimated by $\sqrt{\pi D_1 \times 60\ \mathrm{s}} \approx 670$ μm, which is comparable to the size of nucleated bubbles captured in the initial frame (see table 1). In this sense, one can replace t with $(t + t_0)$ in the evaluation where t_0 is a time shift (or the time to experimentally find nucleated bubbles after inserting the glass slide into the water). It is important to note, however, that the calculation of DN supersaturation

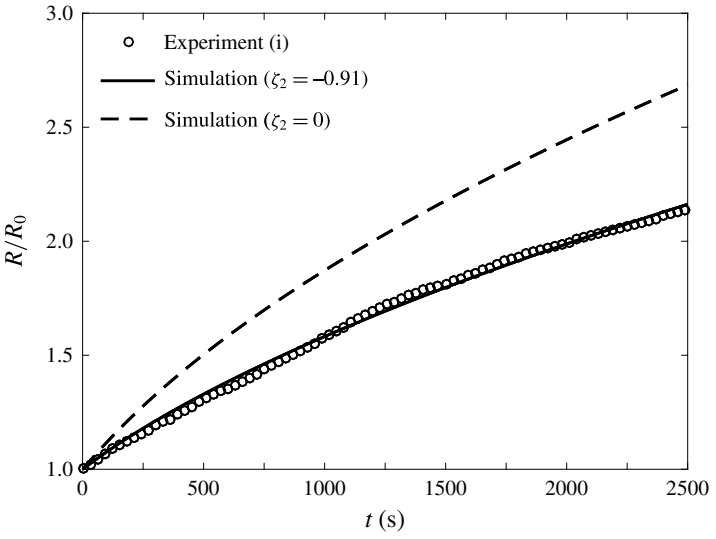

FIGURE 4. Evolution of the growth of the bubble in experiment (i) under the maximum supersaturation of DO at $\zeta_1 = 6.0$. The experiment (i) is compared with the multi-species Epstein–Plesset formula (§ 3) with different supersaturation of DN at $\zeta_2 = -0.91$ (fitted) and $\zeta_2 = 0$.

ζ_2 is almost unaffected by the time shift from the experiments. This means that the boundary layer development is properly evaluated even with the convenient definition of $t = 0$ from the bubble growth visualization (figure 3), as the overall observation period (up to bubble detachment from the glass surface) is two orders of magnitude higher than the initial stage of the boundary layer development (where the boundary layer thickness is smaller than or comparable to bubble radii).

4. Results and discussion

4.1. *Experimental observation*

First, we examine the growth of a surface-attached bubble in experiment (i) under the maximum supersaturation of DO at $\zeta_1 = 6.0$ in figure 3; the measured evolution of the (area-equivalent) bubble radius is plotted with symbols in figure 4; the bubble radius keeps increasing, while its growth is decelerating, as time progresses.

It is of interest to compare this observation with the growth of surface-attached bubbles under CO_2 supersaturation. Since CO_2 has much higher solubility than O_2, a difference in the solution density across the concentration boundary layer that forms from nucleated bubbles will come into play during the long observation of the bubble growth. To be precise, the solution within the boundary layer is CO_2-depleted and its density is thus lower, thereby triggering ascending fluid motion (under buoyancy) around the bubbles. Such natural convection leads to enhancement of the bubble growth rate, for example, in the experiment of Enríquez *et al.* (2014) where the gradual growth driven by diffusion is first observed and the accelerated growth is then obtained after the natural convection onset.

The extent of the density difference is much lower in our case of O_2 because of its low solubility, so, on the contrary, the natural convection around the bubble is expected to have a minor impact on the bubble growth. We say, in other words, that the growth is controlled dominantly by diffusion. Indeed, the time for the natural

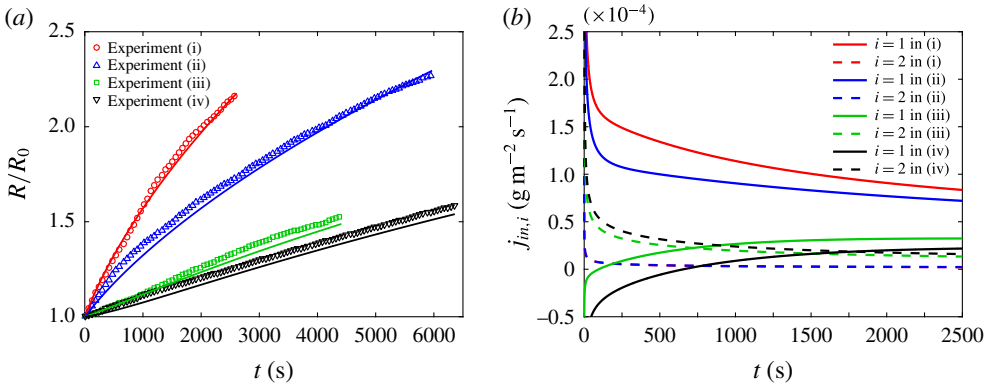

FIGURE 5. (*a*) Evolution of the growth of the bubble in experiments (i)–(iv). These measurements are compared with the multi-species Epstein–Plesset formula (represented by lines) with the DN concentration fitted (see table 1). (*b*) Simulated evolution of the mass influx of gas species i into the bubble, $j_{in,i}$.

convection onset (Enríquez 2015) is estimated at 1200–2900 s for the O_2–water system in experiments (i)–(iv) and is comparable to the observation period, meaning that the natural convection does not alter the early stage of the diffusion-dominant bubble growth.

4.2. *Comparison to the theory*

Now that advection induced by bubble wall velocity $\dot{R} = \mathrm{d}R/\mathrm{d}t$ is also negligible because of small Péclet number ($Pe = 2R\dot{R}/D_1 < 0.1$), the Epstein–Plesset calculation is expected to work. In figure 4, the evolution of the measured bubble growth in experiment (i) is compared with the multi-species Epstein–Plesset theory. In the Epstein–Plesset calculation, there are two unknown parameters:

(i) the initial mole fraction of oxygen gas inside the bubble, $X_1(0) = n_1(0)/(n_1(0) + n_2(0))$;
(ii) the supersaturation of DN, ζ_2.

Now that the water is supersaturated with DO, it is reasonable to assume that the initial bubble content is mainly oxygen gas; in the calculation, we set $X_1(0) = 1$ as the initial condition. It is instructive to note, however, that the change in $X_1(0)$ is not influential in the calculation, meaning that the overall bubble growth is rather insensitive to the initial gas composition of the nucleated bubble.

For the value of DN supersaturation, we consider two scenarios:

(i) DN is undisturbed by the oxygen aeration and keeps being saturated at 0.8 atm (i.e. $\zeta_2 = 0$) (Wilcock & Battino 1974; Bignell 1987);
(ii) DN is purged by the oxygen aeration and thus is lowered (i.e. $\zeta_2 < 0$).

For the latter case, we infer the value of ζ_2 by fitting between the experiment and the theory. It follows from the comparison in figure 4 that the latter scenario is the case and the fitted DN supersaturation is $\zeta_2 = -0.91$. Note that $\zeta_2 = -1$ means that DN is purged perfectly. This suggests that the DN, which is originally saturated under the atmosphere, is effectively purged by the oxygen aeration.

The fitting procedure is applied to the observation up to bubble detachment in experiments (i)–(iv) (see figure 5*a*). The fitted values of ζ_2 are documented in table 1.

The overall trend in the bubble growth is found to be well fitted by the multi-species theory of Epstein and Plesset. We recorded the bubble growth until the bubble was detached from the glass slide, but did not observe remarkable increases in the growth rate by natural convection as seen in the CO_2–water system of Enríquez *et al.* (2014). It is clear that the bubble growth is suppressed as the DO supersaturation ζ_1 is reduced. More importantly, the DN concentration increases as the DO concentration decreases. Since we obtained the lower DO level by leaving the aerated water open to the atmosphere, the nitrogen gas in the atmosphere again dissolves into the water through its free surface.

We calculate the influx of gas species i into the bubble, $j_{in,i} = M_i(\mathrm{d}n_i/\mathrm{d}t)/(4\pi R^2)$, where M_i is the molecular weight of species i, and plot its evolution in figure 5(*b*). For experiments (i) and (ii) where the DO supersaturation is relatively high, the oxygen influx is dominating over the nitrogen influx (except in the initial stage at which the growth is sensitive to the initial condition $X_1(0)$); the bubble growth is driven mainly by the transfer of DO into the bubble. It is interesting to note, on the contrary, that the negative influx (i.e. outflux) of the DO arises when the DO supersaturation is not sufficiently high as in experiments (iii) and (iv); to be specific, the right-hand side of (3.3) is negative because of $p_i > p_{\infty,i}(\zeta_i + 1)$. As the DN is transferred into the bubble, the mole fraction of oxygen X_1 is reduced so that the influx of the DO is eventually obtained, regardless of the initial condition $X_1(0)$.

4.3. *Supplemental experiments*

So far, we have studied the aeration of water with oxygen microbubbles and its role of purging nitrogen gas originally dissolved in the water. We performed supplemental experiments for the case of the aeration with nitrogen microbubbles. As expected, oxygen originally dissolved in water can be purged by the nitrogen aeration as documented in appendix A.

In all the above experiments, the water we used is originally saturated under the atmosphere. We performed another experiment of applying the oxygen aeration to DN-supersaturated water that is prepared by nitrogen aeration beforehand. As expected, it is possible to obtain the purging effect by applying aeration even to the supersaturated water (see appendix B). Therefore, the DN can be effectively purged by oxygen aeration, regardless of the initial state of dissolved gases in the water.

5. Conclusions

To study whether nitrogen gas originally dissolved in water can be purged by aeration with oxygen microbubbles, we devised a technique to measure the concentration of DN. Oxygen microbubbles were continuously injected into the circulation system of tap water that was originally saturated with gases at one atmosphere or was first aerated with nitrogen microbubbles. The gradual growth of a surface-attached bubble in the aerated water was visualized and was then compared with the extended Epstein–Plesset theory that accounts for mass diffusions of multiple gas species. In the comparison, the (unknown) DN concentration is treated as a fitting parameter. It follows from the fitting that the DN can be effectively purged by the oxygen aeration, regardless of the initial state of dissolved gases in the water. From the supplemental experiments, such a purging effect was confirmed also in the case of aeration with nitrogen microbubbles. We say that these purging effects, which are well known particularly in the food industry and fishery, can be evaluated quantitatively by our technique based on the bubble growth observation and its fitting to the extended Epstein–Plesset theory.

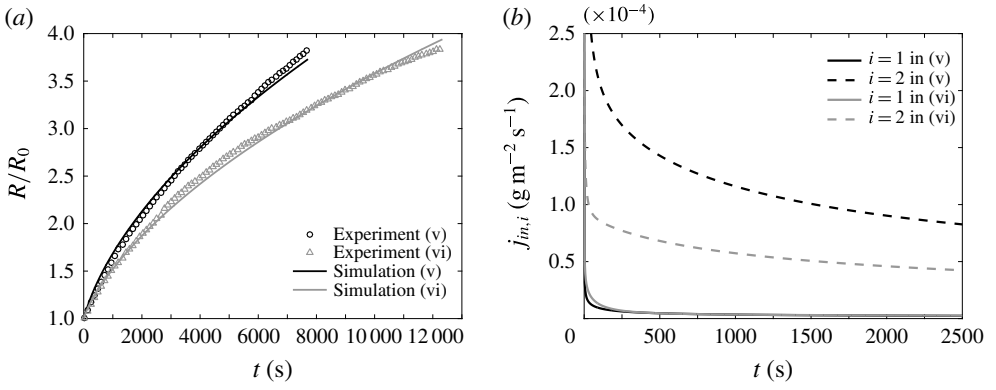

FIGURE 6. (*a*) Evolution of the growth of the bubble in experiments (v) and (vi). These measurements are compared with the multi-species Epstein–Plesset formula with the DN concentration fitted (see table 2). (*b*) Simulated evolution of the mass influx of gas species i into the bubble, $j_{in,i}$.

Experimental condition	(v)	(vi)	(vii)
Initial bubble radius, R_0 (μm)	145	245	214
DO supersaturation (measured), ζ_1	−0.79	−0.7	5.0
DN supersaturation (fitted), ζ_2	2.5	0.86	−0.88

TABLE 2. Initial radius of the nucleated bubble (captured in the initial frame), supersaturation from the DO reading, and fitted values of DN supersaturation in experiments (v)–(vii).

Acknowledgements

We would like to thank the anonymous referees for their insightful comments that enabled us to improve our paper. This work was supported in part by the Mizuho Foundation for the Promotion of Science and by a MEXT Grant-in-Aid for the Program for Leading Graduate Schools.

Appendix A. Nitrogen aeration to air-saturated water

The same experiment as in § 2 is repeated, but aerating with nitrogen bubbles. After the 30 min aeration, the value of ζ_1 decreases to $\min(\zeta_1) = -0.8$ (i.e. DO subsaturation), which means that the DO is effectively purged by the nitrogen aeration. The growth of a surface-attached bubble in the aerated water is then observed; the experimental conditions (v) and (vi) are summarized in table 2.

To detect the supersaturation of DN, we calculate the multi-species Epstein–Plesset equations in § 3 and fit them to the experiments. Since the water is now supersaturated with DN, the bubble just after nucleation is expected to consist mainly of nitrogen gas so that $X_1(0) = 0$; the (unknown) DN supersaturation is treated as a fitting parameter as in § 4.

In figure 6(*a*), the simulated evolution of the bubble growth is compared with the experiments (v) and (vi). The experiments are found to be well fitted to the calculations, meaning that the bubble growth is caused mainly by diffusive effects. At the minimum DO concentration in experiment (v), we predict the maximum

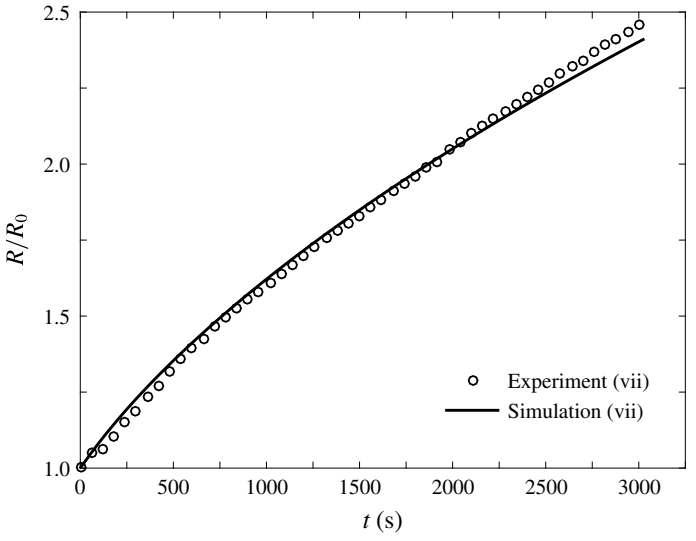

FIGURE 7. As figure 4, but with the oxygen aeration applied to DN-supersaturated water at $\zeta_2 = 1.3$ (fitted according to appendix A).

DN supersaturation at $\max(\zeta_2)$ from the fitting. It should be pointed out that the maximum DO supersaturation obtained from the oxygen aeration is 2.4 times higher than the maximum DN supersaturation from the nitrogen aeration. The evolution of mass influx $j_{in,i}$ in experiments (v) and (vi) is also computed in figure 6(*b*). We can confirm, in this case, that the bubble growth is driven mainly by the transfer of DN into the bubble.

Appendix B. Oxygen aeration to DN-supersaturated water

To examine the influence of the initial state of dissolved gases on the purging performance, we performed another experiment of applying the oxygen aeration to DN-supersaturated water that is prepared by nitrogen aeration beforehand. Aeration with nitrogen microbubbles was first applied to (gas-saturated) tap water for 20 min, producing DO subsaturation at $\zeta_1 = -0.64$ from the DO reading and DN supersaturation at $\zeta_2 = 1.3$ from the analysis as in appendix A. Then, the oxygen aeration was applied to the DN supersaturated water for 30 min. The bubble growth observation and its fitting to the theory followed in figure 7, which allowed us to calculate the DN concentration at $\zeta_2 = -0.88$ (see also table 2) in the water after the oxygen aeration; namely, the dissolved nitrogen was purged effectively as well. We can thus say that the purging effect arises from the aeration, regardless of the initial state of dissolved gases in water.

REFERENCES

BIGNELL, N. 1987 Precise density measurements of aqueous solutions of mixed nonpolar gases. *J. Phys. Chem.* **91** (6), 1687–1690.

BOUCK, G. R. 1980 Etiology of gas bubble disease. *T. Am. Fish. Soc.* **109** (6), 703–707.

BUTLER, I. B., SCHOONEN, M. A. A. & RICKARD, D. T. 1994 Removal of dissolved oxygen from water: a comparison of four common techniques. *Talanta* **41** (2), 211–215.

CHU, S. & PROSPERETTI, A. 2016 History effects on the gas exchange between a bubble and a liquid. *Phys. Rev. Fluids* **1** (6), 064202.

CREECH, J., DIVINO, V., PATTERSON, W., ZALESKY, P. J. & BRENNEN, C. E. 2002 Injection of highly supersaturated oxygen solutions without nucleation. *J. Biomech. Engng* **124** (6), 676–683.

DALVI, S. V. & JOSHI, J. R. 2015 Modeling of microbubble dissolution in aqueous medium. *J. Colloid Interface Sci.* **437**, 259–269.

DUNCAN, P. B. & NEEDHAM, D. 2004 Test of the Epstein–Plesset model for gas microparticle dissolution in aqueous media: effect of surface tension and gas undersaturation in solution. *Langmuir* **20** (7), 2567–2578.

EBINA, K., SHI, K., HIRAO, M., HASHIMOTO, J., KAWATO, Y., KANESHIRO, S., MORIMOTO, T., KOIZUMI, K. & YOSHIKAWA, H. 2013 Oxygen and air nanobubble water solution promote the growth of plants, fishes, and mice. *PLoS One* **8** (6), 2–8.

ENDO, A., SRITHONGOUTHAI, S., NASHIKI, H., TESHIBA, I., IWASAKI, T., HAMA, D. & TSUTSUMI, H. 2008 DO-increasing effects of a microscopic bubble generating system in a fish farm. *Mar. Pollut. Bull.* **57** (1–5), 78–85.

ENRÍQUEZ, O. R. 2015 Growing bubbles and freezing drops: depletion effects and tip singularities. PhD thesis, University of Twente.

ENRÍQUEZ, O. R., HUMMELINK, C., BRUGGERT, G. W., LOHSE, D., PROSPERETTI, A., VAN DER MEER, D. & SUN, C. 2013 Growing bubbles in a slightly supersaturated liquid solution. *Rev. Sci. Instrum.* **84** (6), 065111.

ENRÍQUEZ, O. R., SUN, C., LOHSE, D., PROSPERETTI, A. & VAN DER MEER, D. 2014 The quasi-static growth of CO_2 bubbles. *J. Fluid Mech.* **741**, R1.

EPSTEIN, P. S. & PLESSET, M. S. 1950 On the stability of gas bubbles in liquid–gas solutions. *J. Chem. Phys.* **18** (11), 1505–1509.

GOLDMAN, S. 2007 A new class of biophysical models for predicting the probability of decompression sickness in scuba diving. *J. Appl. Phys.* **103** (2), 484–493.

HOLOCHER, J., PEETERS, F., AESCHBACH-HERTIG, W., KINZELBACH, W. & KIPFER, R. 2003 Kinetic model of gas bubble dissolution in groundwater and its implications for the dissolved gas composition. *Environ. Sci. Technol.* **37** (7), 1337–1343.

KABALNOV, A., KLEIN, D., PELURA, T., SCHUTT, E. & WEERS, J. 1998 Dissolution of multicomponent microbubbles in the bloodstream: 1. Theory. *Ultrasound Med. Biol.* **24** (5), 739–749.

KHUNTIA, S., MAJUMDER, S. K. & GHOSH, P. 2012 Microbubble-aided water and wastewater purification: a review. *Rev. Chem. Engng* **28** (4–6), 191–221.

KOBAYASHI, F., IKEURA, H., OHSATO, S., GOTO, T. & TAMAKI, M. 2011 Disinfection using ozone microbubbles to inactivate *Fusarium oxysporum* f. sp. *melonis* and *Pectobacterium carotovorum* subsp. *carotovorum*. *Crop Prot.* **30** (11), 1514–1518.

KWAN, J. J. & BORDEN, M. A. 2010 Microbubble dissolution in a multigas environment. *Langmuir* **26** (9), 6542–6548.

OTSU, N. 1979 A threshold selection method from gray-level histograms. *IEEE Trans. Syst. Man Cybern.* **SMC-9** (1), 62–66.

PEÑAS-LÓPEZ, P., PARRALES, M. A. & RODRÍGUEZ-RODRÍGUEZ, J. 2015 Dissolution of a CO_2 spherical cap bubble adhered to a flat surface in air-saturated water. *J. Fluid Mech.* **775**, 53–76.

PEÑAS-LÓPEZ, P., PARRALES, M. A., RODRÍGUEZ-RODRÍGUEZ, J. & VAN DER MEER, D. 2016 The history effect in bubble growth and dissolution. Part 1. Theory. *J. Fluid Mech.* **800**, 180–212.

SANDER, R. 2015 Compilation of Henry's law constants (version 4.0) for water as solvent. *Atmos. Chem. Phys.* **15** (8), 4399–4981.

SHIM, S., WAN, J., HILGENFELDT, S., PANCHAL, P. D. & STONE, H. A. 2014 Dissolution without disappearing: multicomponent gas exchange for CO_2 bubbles in a microfluidic channel. *Lab on a Chip* **14** (14), 2428–2436.

TAKAHASHI, M. 2005 Zeta potential of microbubbles in aqueous solutions: electrical properties of the gas–water interface. *J. Phys. Chem.* B **109** (46), 21858–21864.

TERASAKA, K., HIRABAYASHI, A., NISHINO, T., FUJIOKA, S. & KOBAYASHI, D. 2011 Development of microbubble aerator for waste water treatment using aerobic activated sludge. *Chem. Engng Sci.* **66** (14), 3172–3179.

TSUGE, H. 2014 *Micro- and Nanobubbles: Fundamentals and Applications*. CRC.

UESAWA, S., KANEKO, A., NOMURA, Y. & ABE, Y. 2012 Study on bubble breakup in a Venturi tube. *Multiphase Sci. Technol.* **24** (3), 257–277.

WILCOCK, R. J. & BATTINO, R. 1974 Solubility of oxygen–nitrogen mixture in water. *Nature* **252**, 614–615.

WILHELM, E., BATTINO, R. & WILCOCK, R. J. 1977 Low-pressure solubility of gases in liquid water. *Chem. Rev.* **77**, 219–262.

YASUI, K., TUZIUTI, T. & KANEMATSU, W. 2016 Extreme conditions in a dissolving air nanobubble. *Phys. Rev.* E **94** (1), 013106.